International Journal of Numerical Methods for Heat & Fluid Flow

MHD natural convective flow of nanofluids past stationary and moving inclined porous plate considering temperature and concentration gradients with suction

Thirupathi Thumma, A. Chamkha, Siva Reddy Sheri,

MHD natural convective flow of nanofluids past stationary and moving inclined porous plate considering temperature and concentration gradients with suction

Received 9 March 2016
Revised 27 July 2016
Accepted 10 August 2016

Thirupathi Thumma
Department of Mathematics, Padmasri Dr BV Raju Institute of Technology, Narsapur, India

A. Chamkha
Department of Mechanical Engineering, Prince Mohammad Bin Fahd University, Al-Khobar, Saudi Arabia and Prince Sultan Endowment for Energy and Environment, Prince Mohammad Bin Fahd University, Al-Khobar, Saudi Arabia, and

Siva Reddy Sheri
Department of Mathematics, GITAM University, Medak, Telangana, India

Abstract

Purpose – This paper aims to focus on the mathematical modeling of magnetohydrodynamic natural convective boundary layer flow of nanofluids past a stationary and moving inclined porous plate considering temperature and concentration gradients with suction effects.

Design/methodology/approach – The transformed non-dimensional and coupled governing partial differential equations are solved numerically using the finite element method.

Findings – The obtained numerical results for physical governing parameters on the velocity, temperature and concentration distributions are exemplified graphically and presented quantitatively. The boundary layer thickness increased with the increasing values of Soret, Dufour and Grashof numbers, while the thickness of boundary layer decreased with increasing values of suction for both stationary and moving plate cases. The primary and secondary velocity profiles are decreasing with an angle of inclination for moving plate and inclination has no significant effect for the stationary plate. An increase of the Soret number and Dufour number tend to increase the heat and mass transfer, while an increase of suction reduces the heat and mass transfer.

Originality/value – The problem is an important contribution to the field of nanofluid science and technology and is relevant to high temperature rotating chemical engineering systems exploiting magnetized nanofluids. This study is relatively original in nanofluids.

Keywords Nanofluid, Natural convection, Magnetohydrodynamics, Inclined plate, Suction

Paper type Research paper

The authors are thankful for all reviewers for their insightful comments and constructive criticism on this research paper which led to improvements in the quality of the paper scientifically.

International Journal of Numerical Methods for Heat & Fluid Flow
Vol. 27 No. 8, 2017
pp. 1765-1794

0961-5539
DOI 10.1108/HFF-03-2016-0090

Nomenclature

B_0 = Constant applied magnetic field
E = Applied electric field
g = Acceleration due to gravity (ms^{-2})
K = Permeability parameter
k = Permeability of porous medium
k^* = Mean absorption coefficient
M = Dimensionless magnetic field parameter
Nu = Nusselt number
C_f = Skin friction coefficient
Sh = Sherwood number
R = Thermal radiation parameter
Pr = Prandtl number
Sr = Soret number
Du = Dufour number
Gr = Thermal Grashof number
Gc = Solutal Grashof number
α = Angle of inclination
C = Non-dimensional concentration
Sc = Schmidt number
Kr = Chemical reaction parameter
Dm = Coefficient of mass diffusivity (m^2s^{-1})
Kt = Thermal diffusion ratio
Tm = Mean fluid temperature
c_s = Concentration susceptibility
c_p = Specific heat at constant pressure ($JKg^{-1}K^{-1}$)
k^2 = Rotational parameter
Ks = Thermal conductivity of the solid ($Wm^{-1}K^{-1}$)
K_f = Thermal conductivity of the fluid ($Wm^{-1}K^{-1}$)
K_{nf} = Thermal conductivity of the nanofluid ($Wm^{-1}K^{-1}$)
S = Suction parameter
T' = Local temperature of the fluid (K)
T'_w = Wall temperature of the fluid (K)
T'_∞ = Ambient temperature of the fluid (K)
C' = Dimensional concentration (Kgm−3)
C'_w = Concentration at the surface (Kgm^{-3})
C'_∞ = Concentration at free stream (Kgm^{-3})
$w0$ = Normal velocity (ms^{-1})
Ω = Constant angular velocity (ms^{-1})
(x, y, z) = Cartesian coordinates
(u, v, w) = Velocity component along x, z, and y axes (ms^{-1})

Greek symbols

β = Thermal expansion coefficient (K^{-1})
β_f = Coefficient of thermal expansion of the fluid (K^{-1})
β_s = Coefficient of thermal expansion of the solid (K^{-1})
ρ_f = Density of the fluid friction (Kgm^{-3})
ρ_s = Density of the solid friction (Kgm^{-3})
ρ_{nf} = Density of the nanofluid (Kgm^{-3})

v = Kinematic viscosity (m^2s^{-1})
v_f = Kinematic viscosity of the fluid (m^2s^{-1})
μ = Dynamic viscosity (Nsm^{-2})
μ_f = Dynamic viscosity of the fluid (Nsm^{-2})
μ_{nf} = Viscosity of the nanofluid (Nsm^{-2})
σ = Electrical conductivity (Sm^{-1})
σ_s = Electrical conductivity of the solid (Sm^{-1})
σ_f = Electrical conductivity of the fluid (Sm^{-1})
σ_{nf} = Electrical conductivity of the nanofluid (Sm^{-1})
σ^* = Stefan–Boltzmann constant parameter ($5.6697 \times 10\text{-}8\ Wm^{-2}K^{-4}$)
k^* = Mean absorption coefficient
$(\rho c_p)_{nf}$ = Heat capacitance of the nanofluid ($Jm^{-3}K^{-1}$)
$(\rho c_p)_f$ = Heat capacitance of the fluid ($Jm^{-3}K^{-1}$)
ϕ = Volume fraction parameter
ε = Small constant quantity
θ = Non-dimensional temperature

Subscripts
f = Fluid
S = Solid
nf = Nanofluid
w = Condition at the wall
∞ = Condition at free stream

1. Introduction

Nanofluid is the term initially coined by Choi (1995), Choi *et al.* (2001) during an investigation of new class of technologies and coolants at Argonne National Laboratory in the USA, to describe heat transfer fluids that exhibit thermal properties superior to those of their host fluids. Nanofluid is made by suspending nanoparticles (*Cu, Al,* Al_2O_3, TiO_2, *SiC, SiN, AlN*) with average sizes less than 100 nm in conventional heat transfer fluids (H_2O, $C_2H_6O_2$) as well as other base fluids like mineral oil, engine oil and poor heat transfer fluids. During the past decade, the investigation of nanofluid thermal properties attracted immense enthusiasm from research point of view. Thus, the study of particulate suspension has remarkable applications which includes high power X-rays, optical devices, material synthesis, lasers and biomedical science and plenty of possible areas. The introduction and applications of nanofluids can be seen exhaustively in the book by Das *et al.* (2008). Seven slip mechanisms, namely, inertia, Brownian diffusion, thermophoresis, diffusionphoresis, Magnus effect, fluid drainage and gravity in convective transport in nanofluids are investigated by Buongiorno (2006). Recently, by using this model, numerical simulation of natural convection of the nanofluids in heat exchangers were reported by Garoosi *et al.* (2015), and this nanofluid model is adopted by many researchers. However, in this investigation, the nanofluid model proposed by Tiwari and Das (2007) is envisioned.

The combined thermal and mass buoyancy force results the natural convection which has been studied extensively in recent years owing to its broad range of applications in engineering, science and technological processes. Notable applications are the extraction of geothermal energy, the design of pebble bed nuclear reactors, spreading of chemical pollutants in saturated soil food storage and processing, thermal insulation of buildings and many other possible areas. Several investigators studied in free convective boundary layer under various geometries which include permeable vertical cone by Rashad *et al.* (2011), over a horizontal plate by Gorla

and Chamkha (2011) and over convectively heated vertical plate by Aziz and Khan (2012); also, Nield and Kuznetsov (2009) investigated the Cheng–Minkowycz problem for natural convective boundary-layer flow in a porous medium saturated by a nanofluid. Recently by adopting analytical method, revised Cheng–Minkowycz problem for natural convective boundary layer flow of nanofluid in porous medium is investigated by Rashidi *et al.* (2015). The detailed reviews on convective transport in nanofluids have been presented in Abu Nada *et al.* (2010) as well as in the text books by Nield and Bejan (2013) and Ingham and Pop (2005).

From horizontal and vertical surfaces, the natural convection flows in a porous media has been reported by many researchers theoretically and experimentally. Off late, the heat and mass transfer through an inclined plate have gained importance because of, which are encountered in engineering devices such as solar water heaters, chemical processing of heavy metals, electroplating and many more. We have surveyed comprehensively, the technical literature on various aspects of convective flows over an inclined geometries which includes the results on mixed convection in an inclined lid-driven triangular enclosures studied by Rahman *et al.* (2012), along an inclined plate with Brownian motion, and thermophoresis parameter is reported by Rana *et al.* (2012), in an horizontal and inclined tubes with uniform heat flux investigated by Akbari *et al.* (2008), in a lid-driven inclined square enclosures by Abu-Nada and Chamkha (2010) also in natural convection from an inclined plate with internal heat generation or absorption presented by Chamkha *et al.* (2001), with non-uniform wall temperature by Takhar *et al.* (2003), with heat absorption for non-uniform particle phase density by Ramadan and Chamkha (2003) and an analytic solution for particulate suspension by Ramadan and Chamkha (2000). Finally, in the book by Gebhert *et al.* (1988), the work done on natural convection by various authors under different geometries is summarized.

The combined influence of Soret and Dufour effects are significant when species are introduced at a surface in fluid domain. The relations between the driving potentials and fluxes are of high intricate nature. The energy and mass fluxes are caused by means of composition and temperature gradients respectively. These fluxes are also called as diffusion-thermo (Dufour) and thermal-diffusion (Soret) effects. The study of double diffusive natural convection in porous medium has been attracted by many researchers due to enormous applications in engineering and technological processes such as underground disposal of nuclear wastages, bio-chemical contaminants transport in environment, diffusion of medicine in blood, filtration technologies and many more possible areas. It is found from the literature that on double diffusive convection under different geometries which includes the vertical and inclined square cavity (Chamkha and Al-Mudhaf, 2008; Bera and Khalili, 2002; Hossain and Rees, 2003; Chandra Shekar and Kishan, 2015), cylindrical annulus region (Mallikarjuna *et al.*, 2014), truncated cone (Rashad and Chamkha, 2014), vertical slender cylinder (El-Kabeir and Chamkha, 2013), permeable sphere (El-Kabeir *et al.*, 2010). Furthermore, in most of existing literature, various research investigators reported the Soret and Dufour effects in mixed convection boundary layer flows in rectangular duct, toward stretching surface and over a vertical surface for clear fluids.

The magnetohydrodynamic (MHD) flow and heat transfer in porous medium has gained interest due to the effect of rotation and magnetic field on boundary layer. The theory of rotating fluids (Greenspan, 1969) is important, and MHD flow has also attracted many researchers in view of its applications which include underground disposal of radioactive waste material, metal casting and liquid metal cooling blankets for fusion reactors, exothermic chemical reactions, geothermal energy extractions and many more. Oztop *et al.* (2012) studied the MHD natural convection in an enclosure from two semi-circular heaters on the bottom wall. Abolbashari *et al.* (2014) presented analytical solution for entropy

analysis for unsteady MHD flow past a stretching permeable surface in a nanofluid. Chamkha and Aly (2010) reported MHD free convective flow of a nanofluid past a vertical plate in the presence of heat generation or absorption effects. Buoyancy and radiation effects on permeable vertical stretching sheet by adopting numerical (Runge–Kutta integration scheme), and analytical Homotopy analysis method (HAM) methods reported by Rashidi *et al.* (2014a, 2014b) and Ellahi (2013) studied the MHD flow of non-Newtonian nanofluid in a pipe. Sheikholeslami *et al.* (2014) investigated magnetic field effect on nanofluid flow and heat transfer in a semi-annulus enclosure by considering the effects of thermophoresis and Brownian motion to get the gradient of nanoparticles volume fraction. Unsteady MHD free convection flow past a vertical permeable flat plate in a rotating frame of reference with constant heat source in a nanofluid studied by Hamad and Pop (2011).

Despite the aforementioned literature have been reported, to the best of authors knowledge, there seems to be no attempts far been undertaken with regard to diffusion-thermo and thermal-diffusion effects for an inclined plate using nanofluids. Thus, the objective of this paper is finite element study on transient MHD natural convective boundary layer flow of nanofluids past a stationary and moving inclined porous plate considering temperature and concentration gradients with suction. In this comprehensive numerical investigation, we used an extensively validated and robust finite element method. We presented the effects of pertinent physical parameters on primary and secondary velocity distributions, temperature and concentration distributions for two water-based nanofluids $Cu–H_2O$ and $Al_2O_3–H_2O$ in the cases of stationary ($\lambda = 0$) and moving ($\lambda = 1$) inclined porous plate. Furthermore, the formulation of the problem and method of solution are presented in Sections 2 and 3, respectively. Results and discussions are reported in Section 4; finally, important results are summarized in conclusion section.

2. Mathematical formulation of the problem

We considered the MHD natural convection flow with heat and mass transfer of an electrically conducting nanofluid past an infinite porous inclined plate with an acute angle ($0° \leq \alpha \leq 90°$) to the vertical in the presence of thermal radiation and uniform suction in a rotating frame of reference. Consider the Cartesian coordinate system in such a way that x^*-axis is along the direction of the inclined plate through which fluid flow is assumed, y^*-axis perpendicular to the x^*-axis and z^*-axis is normal to the x^*y^*-*plane*. The schematic model of the coordinate system and the physical problem are depicted in Figure 1. The inclination angles 0°, 90° *and* $0° < \alpha < 90°$ represent the vertical, horizontal and inclined plates, respectively. A uniform magnetic field of strength B_0 is imposed transversely to the flow, i.e. along y^*-axis. About y^*-axis., the inclined plate is assumed to be in rigid body rotation with constant angular velocity Ω. The inclined plate is moving with the velocity λu_0, λ being a constant. As inclined plate is assumed to be of infinite extent along x^* *and* y^* directions, then all the physical quantities depend on t^* *and* y^* only. It is assumed that flow is driven by the motion of the inclined plate which oscillates with constant frequency n^* in time t^*, so that inclined plate temp oscillates to $T_w{}^* + \varepsilon(T_w{}^* - T_\infty{}^*)\cos n^*t^*$. It is assumed that inclined plate is electrically non-conducting while the fluid is assumed to be gray, absorbing, emitting but not scattering medium. Initially, at time $t^* \leq 0$, inclined plate and fluid are maintained at uniform temperature T_∞^* and uniform concentration C_∞^*. Once the inclined plate starts moving, i.e. *when* $t^* > 0$ along x^*-axis direction against gravitational field the temperature is raised to T_w^* which is higher than the ambient temperature T_∞^*, and the species concentration at the surface is maintained uniform at C_∞^*. It is assumed that no external electric field is applied. In comparison with the external magnetic field applied, it is

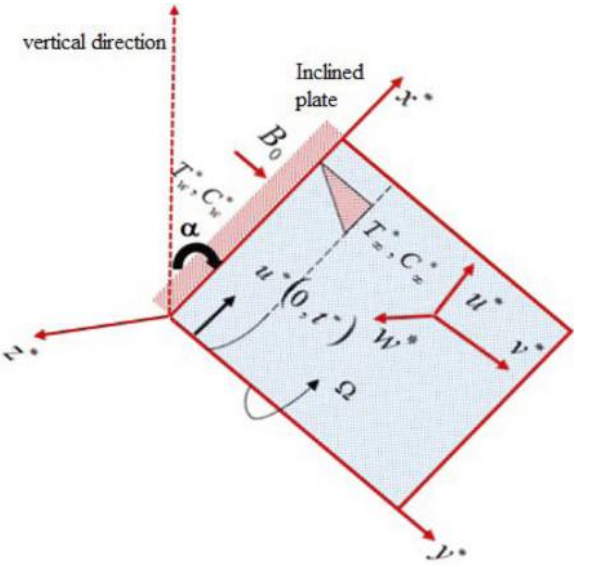

Figure 1.
Schematic diagram of the problem

also assumed that induced magnetic field is negligible so that the magnetic Reynolds number of flow is taken to be very small (Liron and Wilhelm, 1974).

By considering the aforementioned assumptions, the governing boundary layer equations for unsteady natural convective flow under Boussinesq approximations are given by:

$$\frac{\partial w^*}{\partial y^*} = 0 \tag{1}$$

$$\rho_{nf}\left(\frac{\partial u^*}{\partial t^*} + w^*\frac{\partial u^*}{\partial y^*} - 2\Omega v^*\right) = \mu_{nf}\frac{\partial^2 u^*}{\partial y^{*2}} + (g(\rho\beta)_{nf}(T^* - T_\infty^*) + g(\rho\beta)_{nf}(C^* - C_\infty^*))\cos(\alpha) - \sigma_{nf}{B_0}^2 u^* - \frac{v_f u^*}{k} \tag{2}$$

$$\rho_{nf}\left(\frac{\partial v^*}{\partial t^*} + w^*\frac{\partial v^*}{\partial y^*} + 2\Omega u^*\right) = \mu_{nf}\frac{\partial^2 v^*}{\partial y^{*2}} - \sigma_{nf}{B_0}^2 v^* - \frac{v_f v^*}{k} \tag{3}$$

$$(\rho c_p)_{nf}\left(\frac{\partial T^*}{\partial t^*} + w^*\frac{\partial T^*}{\partial y^*}\right) = k_{nf}\frac{\partial^2 T^*}{\partial y^{*2}} - \frac{\partial q_r}{\partial y^*} + \frac{D_m k_t}{c_s c_p}\frac{\partial^2 C^*}{\partial y^{*2}} \tag{4}$$

$$\left(\frac{\partial C^*}{\partial t^*} + w^*\frac{\partial C^*}{\partial y^*}\right) = D_m\frac{\partial^2 C^*}{\partial y^{*2}} - k_r(C^* - {C_\infty}^*) + \frac{D_m k_t}{{T^*}_m}\frac{\partial^2 T^*}{\partial y^{*2}} \tag{5}$$

The corresponding initial and boundary conditions (Ishigaki, 1970; Ganapathy, 1994; Das *et al.*, 2015) on the inclined surface and in free stream can be defined as:

$$\left.\begin{array}{lll} for\ t^* \le 0 & \left\{\begin{array}{ll} \forall y^* & u^*(y^*,t^*)=0,\quad v^*(y^*,t^*)=0,\quad T^*=T^*_\infty, C^*=C^*_\infty \\ y^*=0 & u^*(0,t^*)=\lambda u_0, v^*(0,t^*)=0, \\ & T'(0,t^*)=T^*_w+\varepsilon\left(T^*_w-T^*_\infty\right)\cos n^*t^*,\ C^*=C^*_w \end{array}\right. \\ for\ t^* > 0 & \left\{\begin{array}{ll} y^* \to \infty & u^*(\infty,t^*)\to 0,\quad v^*(\infty,t^*)\to 0,\quad T^*(\infty,t^*)\to T^*_\infty, C^*(\infty,t^*)\to C^*_\infty \end{array}\right. \end{array}\right\} \tag{6}$$

where the direction of the motion of the inclined plate is dented with λ which includes the two values 0 and 1 which used to represent the stationary and upward motion states of inclined plate and u^*, v^* are velocity components along x^* and z^*directions, respectively.

The nanofluid properties (Oztop and Abu-Nada, 2008) are given by:

$$\left.\begin{array}{l} \mu_{nf}=\dfrac{\mu_f}{(1-\varphi)^{2.5}},\ \rho_{nf}=(1-\varphi)\rho_f+\varphi\rho_s,\ (\rho c_p)_{nf}=(1-\varphi)(\rho c_p)_f+\varphi(\rho c_p)_s \\ \sigma_{nf}=\sigma_f\left[1+\dfrac{3(\sigma-1)\varphi}{(\sigma+2)-(\sigma-1)\varphi}\right](\rho\beta)_{nf}=(1-\varphi)(\rho\beta)_f+\varphi(\rho\beta)_s \\ K_{nf}=K_f\left[\dfrac{K_s+2K_f-2\varphi\left(K_f-K_s\right)}{K_s+2K_f+2\varphi\left(K_f-K_s\right)}\right],\ \sigma=\dfrac{\sigma_s}{\sigma_f} \end{array}\right\} \tag{7}$$

The continuity equation $\nabla.\overrightarrow{q}=0$ results in the equation $\frac{\partial w^*}{\partial y^*}=0$; on integrating, we get $w^*=-w_0$; here, constant w_0 is normal velocity at the inclined plate and q_{y^*} is constant. The net radiative heat flux term (Brewster, 1972) by using the Roseland approximation is given by:

$$q_r=\frac{-4\sigma^*}{3k^*}\frac{\partial T^{*4}}{\partial y^*} \tag{8}$$

where k^* and σ^* are Roseland mean absorption coefficient and Stefan–Boltzmann constant, respectively. It is assumed that the temperature difference within the flow are sufficiently small such that T^{*4} may be expressed as a linear function of the temperature by expanding in a Taylor series about T^*_∞ and neglecting the higher order terms. Thus we have:

$$T^{*4}\cong 4{T_\infty}^{*3}T^*-3{T_\infty}^{*4} \tag{9}$$

Hence, from equation (8), using equation (9), we have:

$$\frac{\partial q_r}{\partial y^*}=-\frac{16\sigma^*{T_\infty}^{*3}}{3k^*}\frac{\partial^2 T^*}{\partial y^{*2}} \tag{10}$$

$$\left.\begin{array}{l} y=\frac{u_o y^*}{v_f},\ u=\frac{u^*}{u_o},\ v=\frac{v^*}{u_o},\ t=\frac{u_o^2 t^*}{v_f}, n=\frac{v n^*}{u_o^2},\ S=\frac{w_o}{u_o},\ K=\frac{\rho_f k u_o^2}{v_f^2},\ Kr=\frac{k_r v_f}{u_o^2},\ k^2=\frac{\Omega v_f}{u_o^2} \\ \theta=\frac{T^*-T_\infty^*}{T_w^*-T_\infty^*},\ C=\frac{C^*-C_\infty^*}{C_w^*-C_\infty^*}, M^2=\frac{\sigma_f B_o^2 v_f}{\rho_f u_o^2}, R=\frac{16\sigma^* T_\infty^{*3}}{3kk^*},\ \mathrm{Pr}=\frac{(\rho c_p)_f v_f}{k_f},\ Sc=\frac{v_f}{D_m}, \\ Gr=\frac{g\beta_f v_f (T_w^*-T_\infty^*)}{u_o^3},\ Gc=\frac{g\beta_f v_f (C_w^*-C_\infty^*)}{u_o^3}, Sr=\frac{D_m K t}{T_m v_f}\frac{(T_w^*-T_\infty^*)}{(C_w^*-C_\infty^*)}, Du=\frac{D_m K t}{c_s c_p v_f}\frac{(C_w^*-C_\infty^*)}{(T_w^*-T_\infty^*)} \end{array}\right\} \tag{11}$$

Substituting the nanofluid properties and above-mentioned dimensionless variables in equations (7), (10) and (11) in the equations (2)-(4), we get the following non-dimensional equations:

$$\frac{\partial u}{\partial t}-S\frac{\partial u}{\partial y}-2k^2 v=A_1\frac{\partial^2 u}{\partial y^2}+(GrA_2\theta+GcA_2C)\cos(\alpha)-A_3\left(M^2+\frac{1}{K}\right)u \tag{12}$$

$$\frac{\partial v}{\partial t}-S\frac{\partial v}{\partial y}+2k^2 u=A_1\frac{\partial^2 v}{\partial y^2}-A_3\left(M^2+\frac{1}{K}\right)v \tag{13}$$

$$\frac{\partial \theta}{\partial t}-S\frac{\partial \theta}{\partial y}=A_4\frac{\partial^2 \theta}{\partial y^2}+Du\left(\frac{\partial^2 C}{\partial y^2}\right) \tag{14}$$

$$\frac{\partial C}{\partial t}-S\frac{\partial C}{\partial y}=\frac{1}{Sc}\frac{\partial^2 C}{\partial y^2}-KrC+Sr\left(\frac{\partial^2 \theta}{\partial y^2}\right) \tag{15}$$

where $A_1=\frac{1}{(1-\varphi)^{2.5}\rho_{nf}}, A_2=\frac{(\rho c_p)_{nf}}{(\rho\beta)_{nf}}, A_3=\frac{\sigma_{nf}}{\rho_{nf}}, A_4=\frac{1}{(\rho c_p)_{nf}\mathrm{Pr}}(K_{nf}+R)$.

Subject to initial and boundary conditions in non-dimensional form are:

$$\left.\begin{array}{ll} for\ t\le 0 & \left\{\begin{array}{ll} \forall y & u(y,t)=0,\ \ v(y,t)=0,\ \ \theta(y,t)=0,\ C(y,t)=0 \\ at\ y=0 & u(0,t)=\lambda, v(0,t)=0,\ \ \theta(0,t)=1+\varepsilon\cos nt, C(0,t)=1 \\ as\ y\to\infty & u(\infty,t)\to 0,\ \ v(\infty,t)\to 0,\ \ \theta(\infty,t)\to 0, C(\infty,t)\to 0 \end{array}\right. \\ for\ t>0 & \end{array}\right\} \tag{16}$$

3. Method of solution

The transformed system of coupled and non-homogeneous dimensionless partial differential equations (12)-(15) under the boundary conditions equation (16) are solved numerically for both momentum, energy and species concentration equations by using the extensively validated and robust method known as finite element method. This method has five fundamental steps. An excellent description of these steps presented in the text books by Reddy (2006) and Bathe (1996) which are:

(1) *Step 1. discretization of the domain*: Here in this steep, the entire domain is divided in to finite number of sub-domains, each sub-domain and end points of it are

termed as finite element and nodes of that finite element, respectively. Collection of such finite elements constituted as finite element mesh.

(2) *Step 2: derivation of the element equations*: The derivation of finite element model of the original equation is given by means of algebraic equations in the unknown parameters which involves three important steps. Details of the finite element approximations are provided in the Appendix.

(3) *Step 3: assembly of element equations*: The stiffness matrices obtained in Step 2 in terms of local nodes in each element are assembled using inter element continuity and equilibrium conditions to obtain the global matrices.

(4) *Step 4: imposition of boundary conditions*: The physical boundary conditions in equation (16) are imposed on these assembled equations.

(5) *Step 5: solution of the assembled equations*: The final matrix equations are solved by using an iterative scheme. Furthermore, it is important to calculate the physical quantities of primary interest, which are the skin friction is given by $C_f = \mu_{nf}\left(\frac{\partial u}{\partial y}\right)_{y=0}$, the rate of the heat transfer in terms of the Nusselt number is given by $Nu = -K_{nf}\left(\frac{\partial \theta}{\partial y}\right)_{y=0}$ and the coefficient of Mass transfer, generally known as Sherwood number is given by $Sh = -\mu_{nf}\left(\frac{\partial C}{\partial y}\right)_{y=0}$.

4. Grid independence study

The grid independence is conducted by dividing the entire domain into successively sized grids 131 × 131, 151 × 151 and 171 × 171. The boundary conditions for y *at* ∞ are replaced by a sufficiently large value where the velocity, temperature and concentration profiles approach to zero. We ran the developed code when the suction parameter $S = 0.5$ for different step sizes, and we found very good agreement between the results for all the profiles, which are shown quantitatively in Table I and are also represented graphically in Figure 2. After many trials, for computational flexibility we imposed $y_{max} = 8$ where $y_{max} \rightarrow \infty$, i.e. external to the momentum, energy and concentration boundary layers, and we adopted for all the computations 151 intervals of equal step size 0.053. At each node, four functions are to be evaluated, so that after assembly of elements, a set of 604 linear algebraic equations are formed,

v: secondary velocity			u: primary velocity			θ: temperature			C: concentration		
Grid sizes											
131	151	171	131	151	171	131	151	171	131	151	171
0	0	0	1	1	1	1	1	1	1	1	1
0.0663	0.0663	0.0663	0.936	0.936	0.936	0.9656	0.9656	0.9656	0.9618	0.9618	0.9618
0.1316	0.1316	0.1316	0.8763	0.8763	0.8763	0.9324	0.9324	0.9324	0.924	0.924	0.924
0.1952	0.1952	0.1952	0.8206	0.8206	0.8206	0.9004	0.9004	0.9004	0.8867	0.8867	0.8867
0.2568	0.2568	0.2568	0.7687	0.7687	0.7687	0.8695	0.8695	0.8695	0.8502	0.8502	0.8502
0.316	0.316	0.316	0.7203	0.7203	0.7203	0.8398	0.8398	0.8398	0.8145	0.8145	0.8145
0.3726	0.3726	0.3726	0.6751	0.6751	0.6751	0.811	0.811	0.811	0.7797	0.7797	0.7797
0.4263	0.4263	0.4263	0.6329	0.6329	0.6329	0.7833	0.7833	0.7833	0.7459	0.7459	0.7459
0.4769	0.4769	0.4769	0.5935	0.5935	0.5935	0.7566	0.7566	0.7566	0.7131	0.7131	0.7131
0.5245	0.5245	0.5245	0.5568	0.5568	0.5568	0.7308	0.7308	0.7308	0.6814	0.6814	0.6814

Table I. Grid independence test for different grid sizes

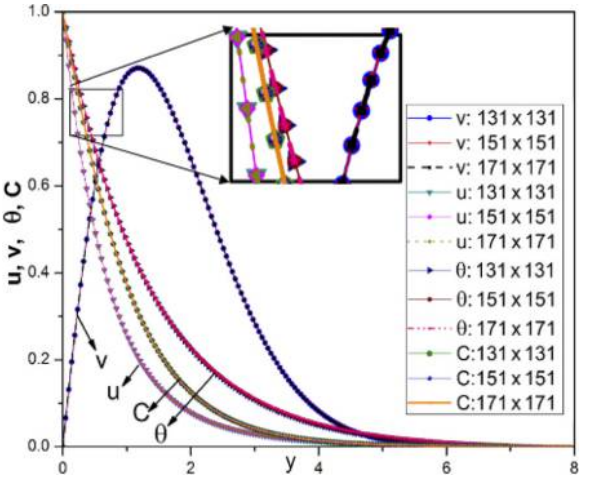

Figure 2.
Grid independence test for primary velocity, secondary velocity, temperature and concentration profiles

consequently an iterative scheme is adopted and by introducing boundary conditions, the system of equations are solved. The solution is assumed to be converged when the difference satisfy the desired accuracy 10^{-7}. Tremendous convergence for all the results is achieved.

5. Results and discussion

The prime aim of this paper is the finite element study on transient natural convective boundary layer MHD flow of nanofluids past a stationary and moving inclined porous plate considering temperature and concentration gradients with suction. Additionally, the influence of *S*, α,*Sr, Du, Gr, Gc, Kr*, k_2, M_2, *K*, *Sc and Pr* on the nanofluid velocity, temperature and species concentration as well as the skin friction, Nusselt number distributions for $Cu–H_2O$ and $Al_2O_3–H_2O$ nanofluids are presented graphically in Figures 3-27. In this paper, we presented the results for the above physical parameters by fixing the values $n = 10$, $nt = \pi/2$, $\varepsilon = 0.02$, $t = 0.1$ and $K = 0.5$, and we adopted the default values for finite element computation which are $k^2 = 4$, $S = 1.0$, $M^2 = 1.0$, $Sr = 1.3$, $Du = 1.5$, $Gr = 5$, $Gc = 4$, $\phi = 0.1$, $\alpha = 45°$, $R = 0.5$, $Pr = 6.2$,

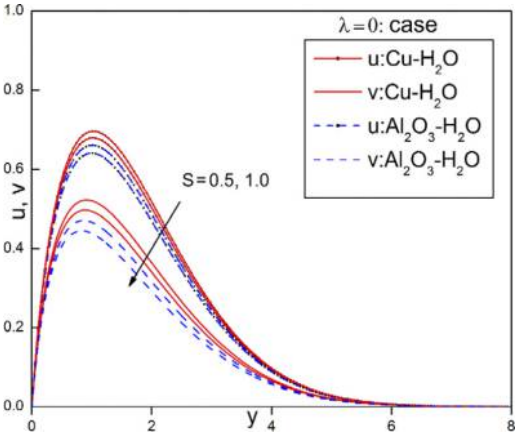

Figure 3.
Effect of suction parameter on dimensionless velocity profiles

Sc = 0.16 and Kr = 0.5. Furthermore, Table II (Oztop and Abu-Nada, 2008) shows thermo physical properties of H_2O, Cu, Ag, Al_2O_3 and TiO_2.

To ascertain the correctness of results obtained through this numerical scheme and MATLAB code, we compared the present results for skin friction and Nusselt number with the results obtained through analytical approach. It should be noted that solution approaches to the solution of Venkateswarlu and Satya Narayana (2015) by considering the constant surface temperature and oscillatory vertical plate, i.e. (α = 0°), velocity without heat generation (Q_H) and absorption (Q_1) terms, which are shown in Table III. We also made comparisons with Hamad and Pop (2011) in the absence of thermal radiation, without heat generation (Q_H) term and mass transfer with (α = 0°), which are shown in Table IV. These comparisons confirm that present results are in admirable agreement with the published reports. Therefore, these favorable comparisons impart the great confidence; subsequently, the developed code can be used in presenting the results quantitatively and graphically.

To present the physical insight of the problem under consideration, two different water-based nanofluids Cu–H_2O and Al_2O_3–H_2O are exemplified graphically for velocity for λ = 0 *and* λ = 1 cases, temperature and concentration profiles. It is worth mentioning here that the momentum boundary layer thickness for Cu–H_2O nanofluid is greater than the other water-based nanofluid Al_2O_3–H_2O, and this is due to fact that the density of copper is more than the alumina. The primary velocity profiles for moving plate starts with the plate velocity and decreased to zero asymptotically at free stream and for stationary plate it raised to

Physical properties	H2O	Cu	Ag	Al2O3	TiO2
Cp(j/kg k)	4,179	385	235	765	686.2
ρ(kg/m3)	997.1	8,933	10,500	3,970	4,250
K(W/m k)	0.613	401	429	40	8.9538
$\beta \times 10^{-5}$(1/k)	21	1.67	1.89	0.85	0.9
σ (S/m)	5.5×10^{-6}	59.6×10^{6}	62.1×10^{6}	35×10^{6}	2.6×10^{6}

Table II. Thermo-physical properties of water and nanoparticles

Pr	Previous results (Venkateswarlu and Satya Narayana, 2015) C_f	Nu	Present results C_f	Nu
0.5	2.3159708	5.9674	2.3159709	5.9674101
1.0	2.2567503	6.0461	2.2567504	6.0461012
1.5	2.1972895	6.1259	2.1972896	6.1259001
2.0	2.1376083	6.2066	2.1376084	6.2066013

Table III. Comparison of skin friction and Nusselt number for various values of pr when ($K \to \infty, \alpha = 0°$, $gr = 0, gc = 0, sr = 0$, $du = 0$)

Pr	Previous results (Hamad and Pop, 2011) C_f	Nu	Present results C_f	Nu
0.5	2.320	5.967	2.3201211	5.9670402
1.0	2.258	6.046	2.2581901	6.0460921
1.5	2.196	6.125	2.1960212	6.1251131
2.0	2.134	6.206	2.1341101	6.2060214

Table IV. Comparison of skin friction and Nusselt number for various values of Pr when ($\alpha = 0°, gr = 0$, $gc = 0, sr = 0, du = 0$)

sharp maximum and then decreased to zero at a distance sufficiently far from the plate surface. Furthermore, the magnitude of the secondary velocity profiles increased to maximum in the momentum boundary layer and decays to asymptotic value with corresponding boundary conditions, and also these profiles are more for the case of $\lambda = 1$ than the case of $\lambda = 0$. Finally, the temperature and concentration profiles for $Cu–H_2O$ is more when we compared with the $Al_2O_3–H_2O$ profiles; this is due to the reason that the high thermal conductivity of Cu than that of Al_2O_3 which in turn leads to the enhancement of the thermal and species concentration boundary layer for $Cu–H_2O$ than the other nanofluids.

The influence of suction on primary velocity and magnitude of the secondary velocity profiles in the cases of stationary and moving plate, are shown in Figures 3 and 4, respectively. These velocity profiles for water-based nanofluids $Cu–H_2O$ and $Al_2O_3–H_2O$ decrease with the increase of the suction parameter S, and this is due to the fact that the suction is induced by drawing nanofluid laterally through the plate surface via pores. This generates an adherence of the nanofluid boundary layer to the plate, destroys momentum in the fluid near the wall surface and consequently stabilizes the boundary layer growth. Therefore, nanofluid momentum boundary layer thickness is suppressed with greater suction. The removal of heat also via lateral mass flux through the plate wall depletes temperatures in the boundary layer as shown in Figure 5. As a result, wall suction can be used effectively for controlling the increase in temperatures and mitigating over-heating of nanomaterial manufacturing processes. Figure 6 demonstrates that nanofluid concentration profiles decrease with the increase of the suction parameter. The deceleration in the flow causes nano-particles of the diffusing species to be drawn nearer to the surface of the plate. This consequently stabilizes the concentration boundary layer growth and decreases nano-particle concentration boundary layer thickness.

The influence of angle of inclination (α) of the surface on primary velocity and magnitude of secondary velocity profiles for moving plate has been depicted in Figures 7 and 8. It is clearly observed from the figures that velocity is decreased with an increase of angle of inclination, and this is due to the fact that drag is experienced at the plate surface. Furthermore, the buoyancy effects decrease due to the thermal diffusion decrease by a factor of gravity components $cos(\alpha)$. Hence, the fluid attains high velocity profiles for the vertical plate than that of inclined. Consequently, momentum boundary layer thickness decrees as a result of decrease in the velocity of nanofluids, which in turn decreases the driving force of the nanofluid.

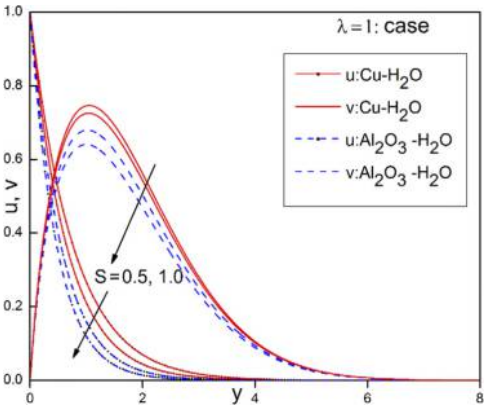

Figure 4.
Effect of suction parameter on dimensionless velocity profiles

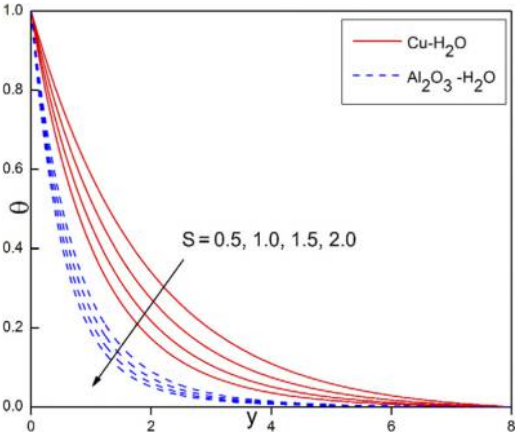

Figure 5.
Effect of suction parameter on dimensionless temperature profiles

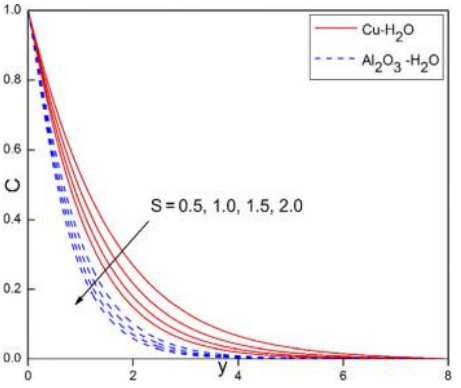

Figure 6.
Effect of suction parameter on dimensionless concentration profiles

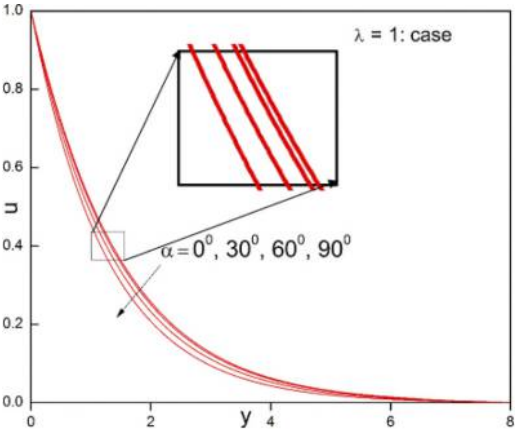

Figure 7.
Effect of inclined angle on dimensionless primary velocity profiles

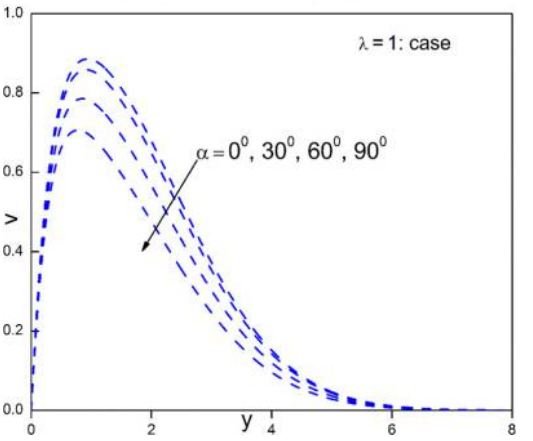

Figure 8.
Effect of inclined angle on dimensionless secondary velocity profiles

Figures 9, 10, 12 and 13 display the increasing of primary velocity and magnitude of the secondary velocity for both the cases of stationary and moving plates with the increasing values of Soret (*Sr*) and (*Du*) Dufour numbers. It is revealed from these graphs that the magnitude of the secondary velocity attains a maximum value near the surface of the boundary layer and then properly reduced to zero at the free stream, and it is more when we compare the case of moving plate with the case of stationary plate. It is also observed from these graphs that the primary velocity profiles attain peak values at the stationary plate surface and then decrease monotonically to zero value satisfying the far field boundary condition and in case of moving plate, primary velocity profiles decrease from plate velocity to free stream value. The concentration profiles against y for different values of Soret number are represented in Figure 11. The contribution of temperature gradients to species diffusion in the flow regime is measured with the Soret number *Sr*. It is evident from the graph that an increase in Soret number causes to increase in concentration profiles which in turn increases the thickness of species concentration boundary layer. This is because, near the plate surface, species concentration is more compared to the concentration at the free

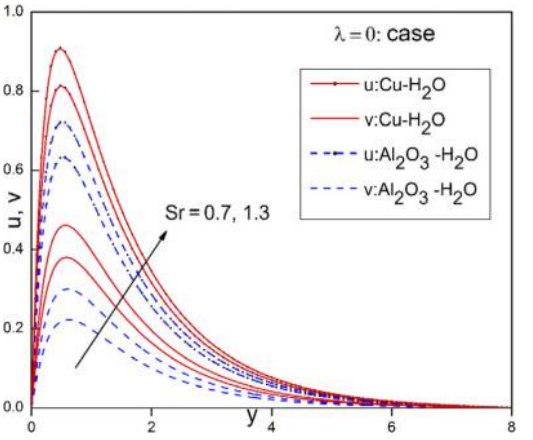

Figure 9.
Effect of Soret number on dimensionless velocity profiles

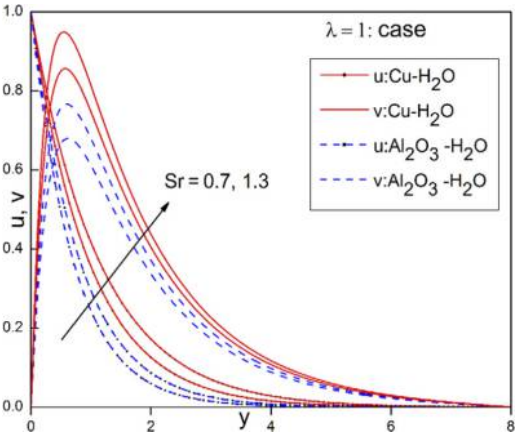

Figure 10.
Effect of Soret number on dimensionless velocity profiles

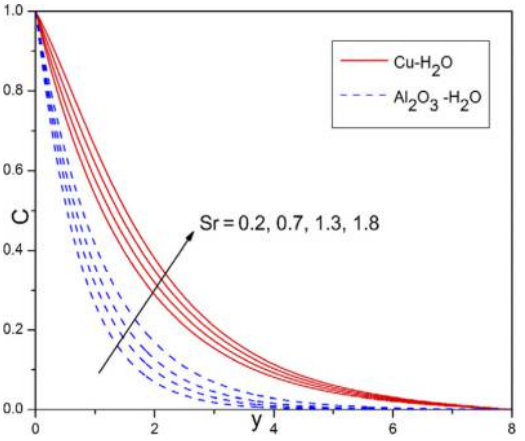

Figure 11.
Effect of Soret number on dimensionless concentration profiles

stream. At the surface, concentration profiles start with the concentration value of the fluid near the plate and then decays monotonically to asymptotic value according to the boundary condition. Finally, the graphs show that the concentration profiles for $Cu–H_2O$ nanofluid is more when we compared to the $Al_2O_3–H_2O$ nanofluid concentration profiles. The influence of Dufour number on temperature distributions is illustrated in Figure 14. The contribution of concentration gradients to thermal energy flux in the flow regime is measured with the Dufour number (*Du*). From the graph, it is noticed that temperature increases with an increase in Dufour number (*Du*) cause to increase in thermal boundary layer thickness. This is due to increase in convective heat exchange at the plate surface. At the surface, fluid temperature profiles start with the temperature of the plate and thereafter temperature decreases monotonically to asymptotic value according to the boundary condition. The thermal Grashof number (*Gr*) is described here as the measure of the relative magnitude of the buoyancy force and the opposing frictional forces acting on the water-based nanofluids. Physically, the positive, negative and zero values of the Grashof number represent the cooling, heating of the boundary surface and absence of free convection currents,

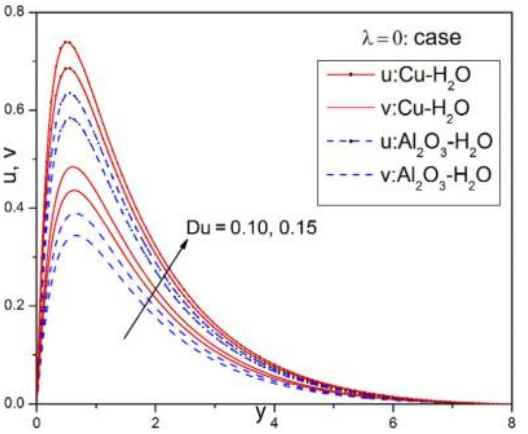

Figure 12.
Effect of Dufour number on dimensionless velocity profiles

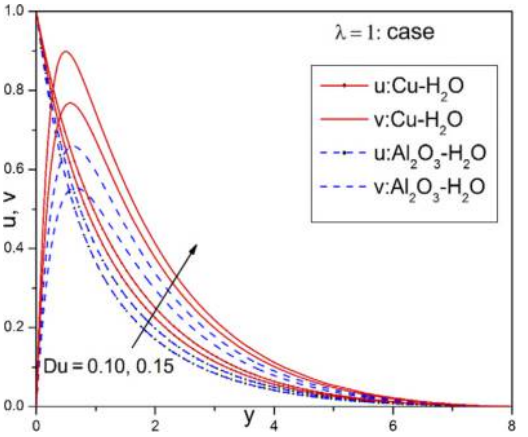

Figure 13.
Effect of Dufour number on dimensionless velocity profiles

respectively. The primary velocity and the magnitude of the secondary velocity profiles for both the cases of stationary and moving plate increase with an increase of thermal Grashof number, and this is due to the dominance of buoyancy forces over the viscous forces, which in turn induces more flow and hence accelerates the fluid velocities. These physical effects are elucidated in Figures 15 and 16. It is evident from the graphs that the shape of the primary velocity and magnitude of the secondary velocity for the case of stationary plate are same but in opposite direction, i.e. the primary and secondary velocity components demonstrate a symmetry about the line $y = 0$. Thermal buoyancy however does not feature in the secondary momentum, and equation (13) implies that the impact on secondary velocity is indirectly experienced via coupling with the primary momentum in equation (12). The secondary flow for the stationary plate case is always reversed as values of v are always negative. For the case of moving plate, the primary velocity starts with the velocity of the plate and gradually decreases to zero at sufficiently far from the boundary layer, and the magnitude of secondary velocity increases with distance from the surface, reaches to

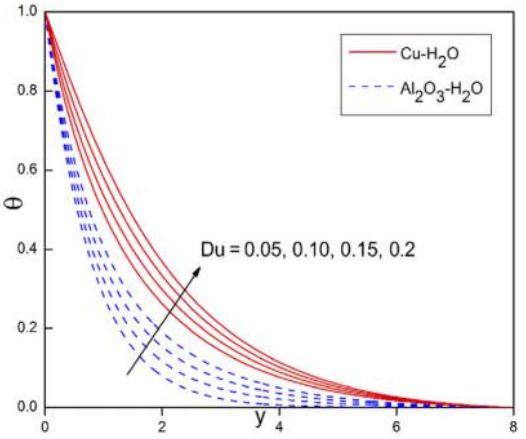

Figure 14.
Effect of Dufour number on dimensionless temperature profiles

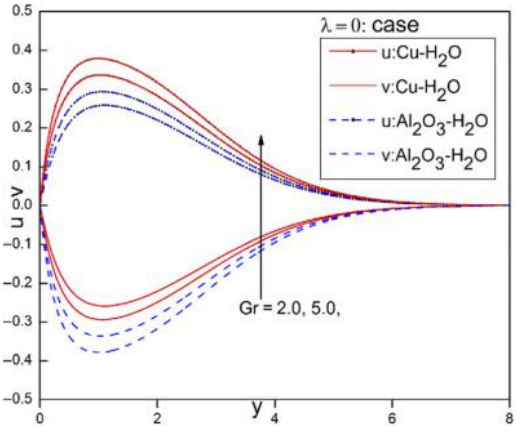

Figure 15.
Effect of thermal Grashof number on dimensionless velocity profiles

maximum value in the vicinity of the plate and decreases monotonically to zero at the free stream.

In the case of stationary and moving plate, increasing the values of the solutal Grashof number (*Gc*), the primary velocity and magnitude of the secondary velocity profiles in the boundary layer are increasing, and are depicted in Figures 17 and 18, and this is agreed from the physical point of view also. The magnitude of the secondary velocity attains a distinctive maximum value in the vicinity of the boundary layer and then settles down to zero at the free stream, and it is more pronounced in the case of moving plate than that of stationary plate. The primary velocity for stationary plate increases sharply, reaches to a maximum value near the surface of the plate and monotonically decreases to the corresponding asymptotic value and for the moving plate it starts with the plate velocity and decays to corresponding asymptotic value. It is also noticed from the graphs that the velocity profiles for $Cu–H_2O$ nanofluid is more when we compared to the $Al_2O_3–H_2O$ nanofluid velocity profiles for both thermal and solutal Grashof numbers; this is because of the higher thermal conductivity of *Cu* than the Al_2O_3.

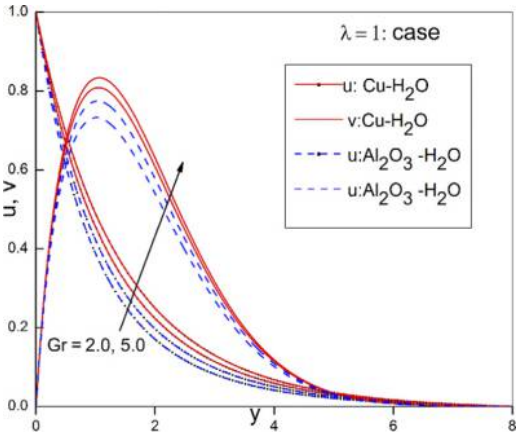

Figure 16.
Effect of thermal Grashof number on dimensionless velocity profiles

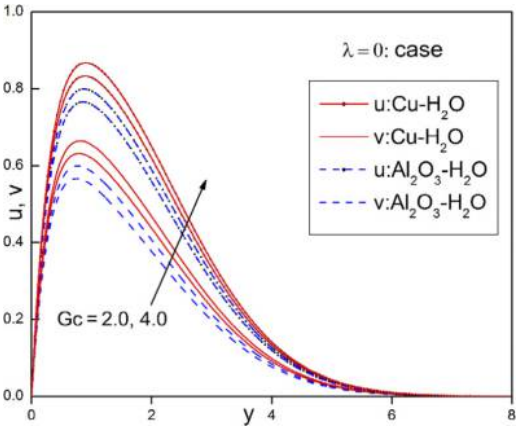

Figure 17.
Effect of solutal Grashof number on dimensionless velocity profiles

The effect of first-order chemical reaction parameter on concentration profiles is displayed in Figure 19. The term $-KrC$ in equation (15) indicates a destructive chemical reaction in which nano-particle species is decreased in the regime for $Kr > 0$. This results in depletion also in nano-particle concentration boundary layer thickness. Therefore, whenever chemical reaction parameter increases, it decelerates the dimensionless concentration profiles. Furthermore, $Cu–H_2O$ is influenced greatly by the Kr than that of $Al_2O_3–H_2O$. Hence, species concentration boundary layer of $Al_2O_3–H_2O$ is lower than the $Cu–H_2O$. The primary velocity and magnitude of the secondary velocity profiles in the cases of stationary and moving plate for different values of rotational parameter k^2 are presented in Figures 20 and 21, in which nanofluid velocity profiles are decrease with the increase of rotational parameter. The rotational parameter features in the Coriolis body force terms arising in both the dimensionless primary momentum equation (12) and the dimensionless secondary momentum equation (13). These terms are $r–2k^2v$ and $+2k^2u$, respectively, and $k^2u = \Omega v_f/u_0^2$ is directly proportional to the angular velocity of the rotating plate. As k^2 is increased, the Coriolis force is also enhanced, i.e. the rotation of the plate is more intense, but

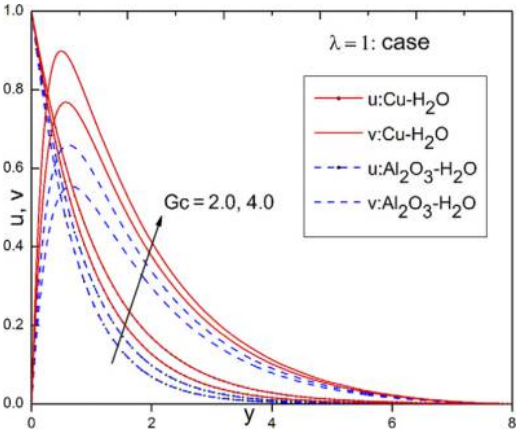

Figure 18.
Effect of solutal Grashof number on dimensionless velocity profiles

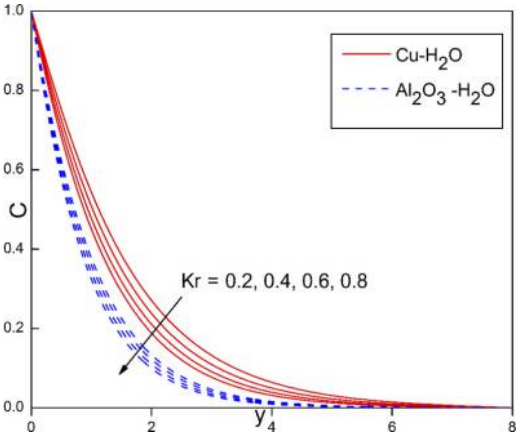

Figure 19.
Effect of chemical reaction parameter on dimensionless concentration profiles

the body force which is negative for primary flow also becomes stronger, and this leads to a significant deceleration in the primary and secondary flow. Although the secondary rotational body force is increased, the dominant effect is that of the primary rotational body force (Coriolis force) which leads to a concurrent deceleration also in the secondary flow, i.e. damping of the flow velocity.

An increase of magnetic field M^2 along the surface causes to decrease the primary velocity and magnitude of the secondary velocity distributions across the momentum boundary layer in the cases of stationary and moving plate and decays to zero asymptotically at the edge of hydrodynamic boundary layer. Thus, boundary layer thickness decreases with the increase of M^2 for water-based nanofluids. This physical phenomenon is due to the reason that an application of transverse magnetic field M^2 to the electrically conducting fluid produces resistive type force, called as Lorentz force, it acts against the relative motion of the fluid. Therefore, this force slows down the motion of the fluid in the boundary layer. This physical behavior is characterized by velocity profiles in

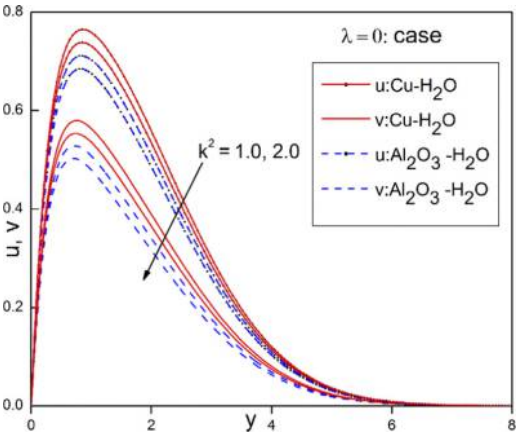

Figure 20.
Effect of rotation parameter on dimensionless velocity profiles

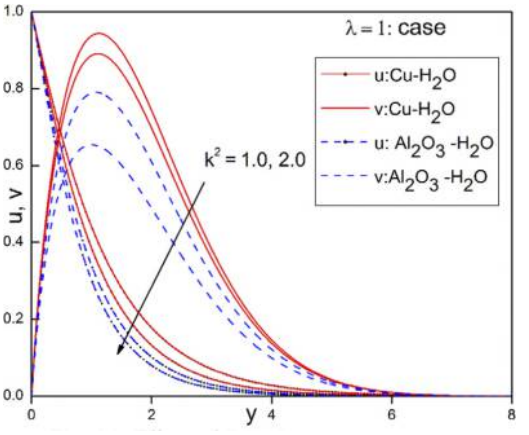

Figure 21.
Effect of rotation parameter on dimensionless velocity profiles

the immediate vicinity of boundary layer as shown in Figures 22 and 23. Porous medium impact is significant on the momentum boundary layer growth; thus, an increase in the permeability parameter K leads to the rise in the fluid flow through the porous medium. This physical behavior is illustrated in Figures 24 and 25. These graphs show the effect of permeability parameter on the primary velocity and magnitude of the secondary velocity distributions for stationary and moving inclined plate cases for two water-based nanofluids. As K increases, the nanofluid velocity profiles increases; thus, the momentum boundary layer thickness increases with K.

The Schmidt number is the ratio of the momentum diffusivity to the mass (species) diffusivity, i.e. it relates the thickness of the hydrodynamic boundary layer to that of the concentration boundary layer. The dimensionless concentration profiles are shown in Figure 26 for various values of the Schmidt number (Sc) and the values of Schmidt number are chosen to represent the presence of species by rare-gas (0.45), water-vapor (0.62), ammonia (0.78) and propyl benzene (2.62) at $25°C$ temperature and 1 atmospheric pressure. From this figure, it is observed that the concentration profiles are decreased as the Schmidt

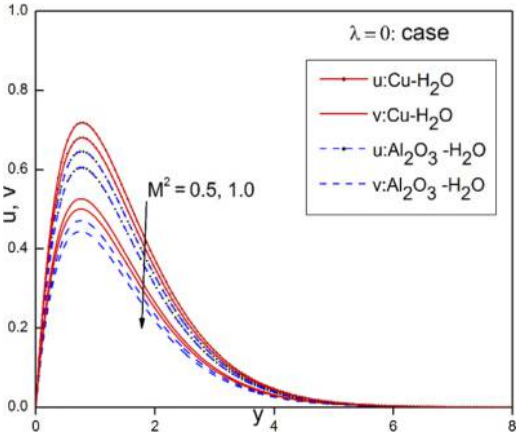

Figure 22.
Effect of magnetic field parameter on dimensionless velocity profiles

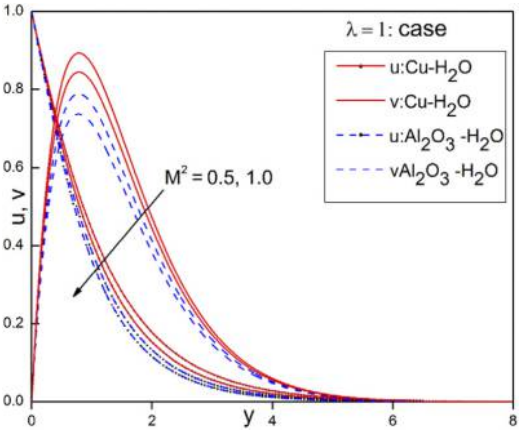

Figure 23.
Effect of magnetic field parameter on dimensionless velocity profiles

number is increased. Due to chemical species, molecular diffusivity is decreased whenever the Schmidt number is increased. Therefore, the concentration boundary layer thickness decreases as the Schmidt number increases. The variations in the temperature profiles for different values of Prandtl number Pr are depicted in Figure 27. Prandtl number refers to the relative contribution of momentum diffusion to thermal diffusion in the boundary layer regime. Furthermore, an increase in the Prandtl number results in a decrease in the temperature distribution in the thermal boundary layer. The physical reason is that smaller values of Pr are equivalent to an increasing thermal conductivity, and therefore, heat is able to diffuse away from the heated surface more rapidly than at higher values of Pr. Hence, the rate of heat transfer is reduced. Therefore, an increase in the value of Pr causes a reduction in the thickness of the thermal boundary layer.

Conclusions

A finite element model is formulated to study the transient MHD natural convective boundary layer flow of nanofluids past a stationary and moving inclined porous plate

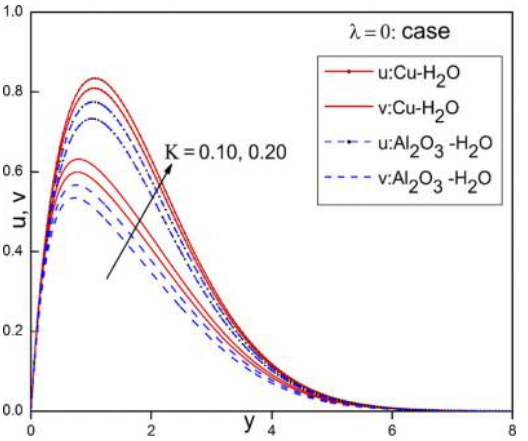

Figure 24.
Effect of permeability parameter on dimensionless velocity profiles

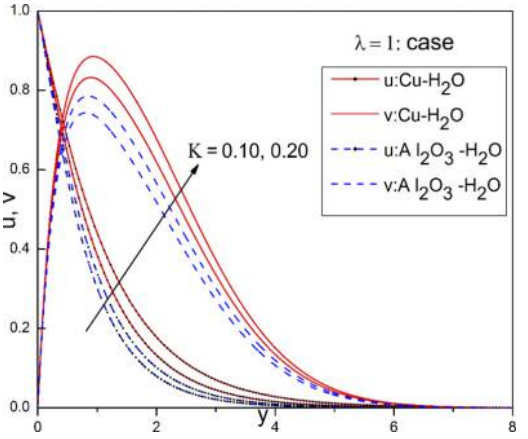

Figure 25.
Effect of permeability parameter on dimensionless velocity profiles

considering temperature and concentration gradients with suction effects. The partial differential equations which governs the flow problem under consideration has been solved numerically by using robust and extensively validated finite element method. The novelty of the present study is the influence of governing parameters on dimensionless velocity for stationary and moving plate cases, temperature and concentration profiles using two different types of water-based nanofluids $Cu–H_2O$ and $Al_2O_3–H_2O$ under oscillatory surface temperature conditions has been presented quantitatively and graphically. Finally, to determine the convergence, accuracy and validity of the code, the results were compared with previously published reports, and an excellent agreement is observed. The summary of significant findings is presented below:

- The boundary layer thickness increased with increasing values of *Sr, Du*, *Gr and Gc*, while the thickness of boundary layer decreased with increasing values of k^2, *S and* M^2 for both stationary and moving plate cases. The primary and secondary velocity profiles are decreasing with an angle of inclination α for moving plate, and it should be noticed that inclination has no significant effect for stationary plate. It is

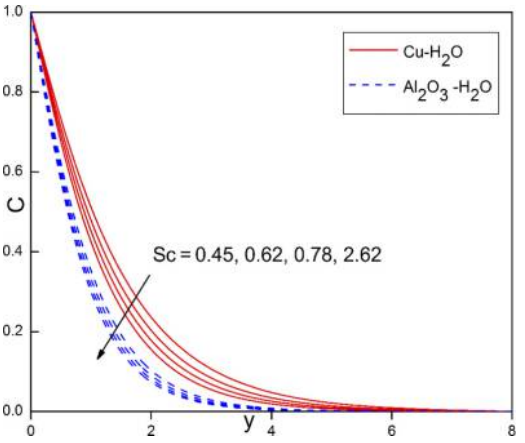

Figure 26.
Effect of Schmidt number on dimensionless concentration profiles

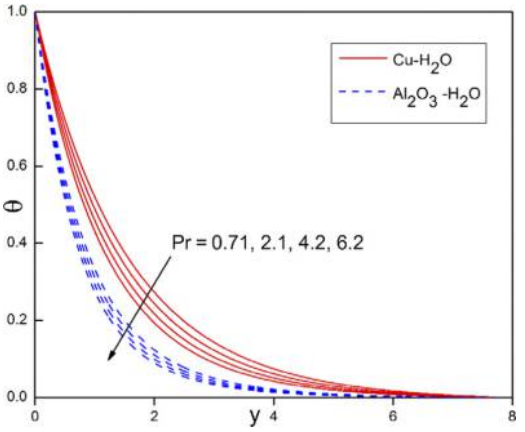

Figure 27.
Effect of Prandtl number on dimensionless temperature profiles

worth mentioning here that $Cu–H_2O$ nanofluid velocity distributions attains zero velocity asymptotically faster than the $Al_2O_3–H_2O$ nanofluid; this is due to the reason that momentum boundary layer for $Cu–H_2O$ nanofluid is thinner than the momentum boundary layer of $Al_2O_3–H_2O$ nanofluid.

- An increase of physical parameters *R and Du* tends to increase the thickness of the thermal boundary layer, while the other parameters *S* and Pr reduce the thickness of thermal boundary layer. The species concentration boundary layer increases with an increase of *Sr*, while the increasing parameters *Sc*, *S* and *Kr* leads to decelerate the concentration boundary layer.
- Furthermore, the thickness of thermal and concentration boundary layer of $Cu–H_2O$ is relatively more when we compare the thickness of thermal and concentration boundary layer of $Al_2O_3–H_2O$ nanofluid. Finally, the influence of thermal-diffusion and diffusion-thermo effects are significant in heat and mass transfer of water-based nanofluids.

References

Abolbashari, M.H., Freidoonimehr, N., Nazari, F. and Rashidi, M.M. (2014), "Entropy analysis for an unsteady MHD flow past a stretching permeable surface in a nanofluid", *Powder Technology*, Vol. 267, pp. 256-267.

Abu-Nada, E. and Chamkha, A.J. (2010), "Mixed convection flow in a lid-driven inclined square enclosures filled with a nanofluid", *European Journal of Mechanics B/Fluids*, Vol. 29 No. 6, pp. 472-482.

Abu Nada, E., Masoud, Z., Oztop, H.F. and Campo, A. (2010), "Effect of nanofluid variable properties on natural convection in enclosures", *International Journal of Thermal Sciences*, Vol. 49 No. 3, pp. 479-491.

Akbari, M., Behzadmehr, A. and Shahraki, F. (2008), "Fully developed mixed convection in horizontal and inclined tubes with uniform heat flux using nanofluid", *International Journal of Heat and Fluid Flow*, Vol. 29 No. 2, pp. 545-556.

Aziz, A. and Khan, W.A. (2012), "Natural convective boundary layer flow of a nanofluid past a convectively heated vertical plate", *International Journal of Thermal Sciences*, Vol. 52, pp. 83-90.

Bathe, K.J. (1996), *Finite Element Procedures*, Prentice-Hall, NJ.

Bera, P. and Khalili, A. (2002), "Double-diffusive natural convection in an anisotropic porous cavity with opposing buoyancy forces: multi solutions and oscillations", *International Journal of Heat and Mass Transfer*, Vol. 45 No. 15, pp. 3205-3222.

Brewster, M.Q. (1972), *Thermal Radiative Transfer Properties*, Wiley, Hoboeken, NJ.

Buongiorno, J. (2006), "Convective transport in nanofluids", *Journal of Heat Transfer*, Vol. 128 No. 3, pp. 240-250.

Chamkha, A.J. and Al-Mudhaf, A. (2008), "Double-diffusive natural convection inclined porous cavities with various aspect ratios and temperature-dependent heat source or sink", *Heat and Mass Transfer*, Vol. 44 No. 6, pp. 679-693.

Chamkha, J. and Aly, A.M. (2010), "MHD free convection flow of a nanofluid past a vertical plate in the presence of heat generation or absorption effects", *Chemical Engineering Communications*, Vol. 198 No. 3, pp. 425-441.

Chamkha, A.J., Rahim, A. and Khaled, A. (2001), "Similarity solutions for hydromagnetic simultaneous heat and mass transfer by natural convection from an inclined plate with internal heat generation or absorption", *Heat and Mass Transfer*, Vol. 37 No. 2, pp. 117-123.

Chandra Shekar, B. and Kishan, N. (2015), "Soret and Dufour effects on free convective heat and solute transfer in fluid saturated inclined porous cavity", *Engineering Science and Technology, an International Journal*, Vol. 18 No. 4, pp. 543-554.

Choi, S. (1995), "Enhancing thermal conductivity of fluids with Nanoparticles, in developments and Applications of non-Newtonian flows", in Siginer, D.A. and Wang, H.P. (Eds), *ASME International Mechanical Engineering Congress & Exposition*, San Francisco, CA, 12-17 November, pp. 66: 99-105.

Choi, S.U.S., Zhang, Z.G., Yu, W., Lockwood, F.E. and Grulke, E.A. (2001), "Anomalously thermal conductivity enhancement in nanotube suspensions", *Applied Physics Letters*, Vol. 79 No. 14, p. 2252.

Das, S., Jana, R.N. and Chamkha, A.J. (2015), "Magnetohydrodynamic free convective boundary layer flow of nanofluids past porous plate in a rotating frame", *Journal of Nanofluids*, Vol. 4 No. 2, pp. 176-185.

Das, S.K., Choi, S.U.S., Yu, W. and Pradeep, T. (2008), *Nanofluids: Science and Technology*, Wiley, NJ.

El-Kabeir, S.M.M. and Chamkha, A.J. (2013), "Heat and mass transfer by mixed convection from a vertical slender cylinder with chemical reaction and soret and dufour effects", *Heat Transfer-Asian Research*, Vol. 42 No. 7, pp. 618-629.

El-Kabeir, S.M.M., Chamkha, A.J., Rashad, A.M. and Al-Mudhaf, H.F. (2010), "Soret and Dufour effects on heat and mass transfer by non-Darcy convection from a permeable sphere embedded in a high porosity medium with chemically reactive species", *International Journal of Energy and Technology*, Vol. 2 No. 18, pp. 1-10.

Ellahi, R. (2013), "The effects of MHD and temperature dependent viscosity on the flow of non-newtonian nanofluid in a pipe: analytical solutions", *Applied Mathematical Modelling*, Vol. 37 No. 3, pp. 1451-1467.

Ganapathy, R. (1994), "A note on oscillatory couette flow in a rotating system", *Journal of Applied Mechanics*, Vol. 61 No. 1, pp. 208-209.

Garoosi, F., Jahanshaloo, L., Rashidi, M.M., Badakhsh, A. and Ali, M.A. (2015), "Numerical simulation of natural convection of the nanofluid in heat exchangers using a buongiorno model", *Applied Mathematics and Computation*, Vol. 254, pp. 183-203.

Gebhert, B., Jaluria, Y., Mahajan, R.L. and Sammakia, B. (1988), *Buoyancy-Induced Flows and Transport*, Hemisphere, New York, NY.

Gorla, R.S.R. and Chamkha, A. (2011), "Natural convective boundary layer flow over a horizontal plate embedded in a porous medium saturated with a nanofluid", *Journal of Modern Physics*, Vol. 2 No. 2, pp. 62-71.

Greenspan, H.P. (1969), *The Theory of Rotating Fluids*, Cambridge University Press, London.

Hamad, M.A.A. and Pop, I. (2011), "Unsteady MHD free convection flow past a vertical permeable flat plate in a rotating frame of reference with constant heat source in a nanofluid", *Heat and Mass Transfer*, Vol. 47 No. 12, pp. 1517-1524.

Hossain, M.A. and Rees, D.A.S. (2003), "Natural convection flow of viscous incompressible fluid in a rectangular porous cavity heated from below the cold side walls", *Heat Mass Transfer*, Vol. 39, Nos 8/9, pp. 657-663.

Ingham, D.B. and Pop, I. (2005), *Transport Phenomena in Porous Media III*, Elsevier, Oxford.

Ishigaki, H. (1970), "Periodic boundary layer near a two-dimensional stagnation point", *Journal of Fluid Mechanics*, Vol. 43 No. 3, pp. 477-486.

Liron, N. and Wilhelm, H.E. (1974), "Integration of the magnetohydrodynamic boundary layer equation by Meksyn's method", *ZAMM – (Zeitschrift für Angewandte Mathematik und Mechanik)*, Vol. 54 No. 1, pp. 27-37.

Mallikarjuna, B., Chamkha, A.J. and Bhuvana Vijaya, R. (2014), "Soret and Dufour effects on double-diffusive convective flow through a non-Darcy porous medium in a cylindrical annulus region in the presence of heat sources", *Journal of Porous Media*, Vol. 17 No. 7, pp. 623-636.

Nield, D.A. and Bejan, A. (2013), *Convection in Porous Media*, 4th ed., Springer, New York, NY.

Nield, D.A. and Kuznetsov, A.V. (2009), "The Cheng–Minkowycz problem for natural convective boundary-layer flow in a porous medium saturated by a nanofluid", *International Journal of Heat and Mass Transfer*, Vol. 52 Nos 25/26, pp. 5792-5795.

Oztop, H.F. and Abu-Nada, E. (2008), "Numerical study of natural convection in partially heated rectangular enclosures filled with nanofluids", *International Journal of Heat and Mass Transfer*, Vol. 29 No. 5, pp. 1326-1336.

Oztop, H.F., Rahman, M.M., Ahsan, A., Hasanuzzaman, M., Saidur, R., Al-Salem, K.H. and Rahim, N.A. (2012), "MHD natural convection in an enclosure from two semi-circular heaters on the bottom wall", *International Journal of Heat Mass Transfer*, Vol. 55 Nos 7/8, pp. 1844-1854.

Rahman, M.M., Oztop, H.F., Ahsan, A., Saidur, R., Al-Salem, K. and Rahim, N.A. (2012), "Laminar mixed convection in inclined triangular enclosures filled with water based cu nanofluid", *Industrial & Engineering Chemistry Research*, Vol. 51 No. 10, pp. 4090-4100.

Ramadan, H.M. and Chamkha, A.J. (2000), "Analytical solutions for hydromagnetic free convection of a particulate suspension from an inclined plate with heat absorption", *International Journal of Fluid Mechanics Research*, Vol. 27 Nos 2/4, pp. 447-467.

Ramadan, H.M. and Chamkha, A.J. (2003), "Hydromagnetic free convection of a particle suspension from a permeable inclined plate with heat absorption for non-uniform particle-phase density", *Heat and Mass Transfer*, Vol. 39 No. 5, pp. 367-374.

Rana, P., Bhargava, R. and Beg, O.A. (2012), "Numerical solution for mixed convection boundary layer flow of a nanofluid along an inclined plate embedded in a porous medium", *Computers and Mathematics with Applications*, Vol. 64 No. 9, pp. 2816-2832.

Rashad, A. and Chamkha, A. (2014), "Heat and mass transfer by natural convection flow about truncated cone in porous media with Soret and Dufour", *International Journal of Numerical Methods for Heat & Fluid Flow*, Vol. 24 No. 3, pp. 595-612.

Rashad, A.M., El-Hakiem, M.A. and Abdou, M.M.M. (2011), "Natural convection boundary layer of a non- newtonian fluid about a permeable vertical cone embedded in a porous medium saturated with a nanofluid", *Computers & Mathematics with Applications*, Vol. 62 No. 8, pp. 3140-3151.

Rashidi, M.M., Rostami, B., Freidoonimehr, N. and Abbasbandy, S. (2014b), "Free convective heat and mass transfer for MHD fluid flow over a permeable vertical stretching sheet in the presence of the radiation and buoyancy effects", *AIN Shams Engineering Journal*, Vol. 5, pp. 901-912.

Rashidi, M.M., Shamekhi, L., Basiripasra, A. and Momoniat, E. (2015), "Entropy generation analysis of the revised Cheng-Minkowycz problem for natural convective boundary layer flow of nanofluid in a porous medium using an analytical method", *Thermal Science*, Vol. 19 No. 1, p. 169.

Rashidi, M.M., Vishnu Ganesh, N., Abdul Hakeem, A.K. and Ganga, B. (2014a), "Buoyancy effects on MHD flow of nanofluids over a stretching sheet in the presence of thermal radiation", *Journal of Molecular Liquids*, Vol. 198, pp. 234-238.

Reddy, J.N. (2006), *An Introduction to the Finite Element Method*, 3rd ed., McGraw-Hill Book Company, New York, NY.

Sheikholeslami, M., Gorji-Bandpy, M., Ganji, D.D., Rana, P. and Soleimani, S. (2014), "Magnetohydrodynamic free convection of Al_2O_3-water nanofluid considering thermophoresis and Brownian motion effects", *Computers & Fluids*, Vol. 94, pp. 147-160.

Takhar, H.S., Chamkha, A.J. and Nath, G. (2003), "Effects of non-uniform wall temperature or mass transfer in finite sections of an inclined plate on the MHD natural convection flow in a temperature stratified high porosity medium", *International Journal of Thermal Sciences*, Vol. 42 No. 9, pp. 829-836.

Tiwari, R.K. and Das, M.K. (2007), "Heat transfer augmentation in a two-sided lid-driven differentially heated square cavity utilizing nanofluids", *International Journal Heat Mass Transfer*, Vol. 50 Nos 9/10, pp. 2002-2018.

Venkateswarlu, B. and Satya Narayana, P.V. (2015), "Chemical reaction and radiation absorption effects on the flow and heat transfer of a nanofluid in a rotating system", *Applied Nanoscience*, Vol. 5 No. 3, pp. 351-360, doi: 10.1007/s1320-014-0324-3.

Appendix

Construction of the variational formulation of the differential equations

The variational formulation associated with equations (12)-(15) over a typical two-node linear element $(y_e,\ y_{e+1})$ is given by:

$$\int_{y_e}^{y_{e+1}} w_1\left[\frac{\partial u}{\partial t} - S\left(\frac{\partial u}{\partial y}\right) - A_1\left(\frac{\partial^2 u}{\partial y^2}\right) - 2k^2 v - A_2(Gr\theta + GcC)\cos(\alpha) + A_3\left[M^2 + \frac{1}{K}\right]u\right]dy = 0 \tag{17}$$

$$\int_{y_e}^{y_{e+1}} w_2\left[\frac{\partial v}{\partial t} - S\left(\frac{\partial v}{\partial y}\right) - A_1\left(\frac{\partial^2 v}{\partial y^2}\right) + 2k^2 u + A_3\left[M^2 + \frac{1}{K}\right]v\right]dy = 0 \tag{18}$$

$$\int_{y_e}^{y_{e+1}} w_3\left[\frac{\partial \theta}{\partial t} - S\left(\frac{\partial \theta}{\partial y}\right) - A_4\left(\frac{\partial^2 \theta}{\partial y^2}\right) - Du\frac{\partial^2 C}{\partial y^2}\right]dy = 0 \tag{19}$$

$$\int_{y_e}^{y_{e+1}} w_4\left[\frac{\partial C}{\partial t} - S\left(\frac{\partial C}{\partial y}\right) - \frac{1}{Sc}\left(\frac{\partial^2 C}{\partial y^2}\right) + KrC - Sr\frac{\partial^2 \theta}{\partial y^2}\right]dy = 0 \tag{20}$$

where W_1, W_2, W_3 and W_4 are arbitrary test functions and may be viewed as the variations in u, v, θ and C, respectively. After reducing the order of integration and non-linearity, we arrive at the following system of equations:

$$\int_{y_e}^{y_{e+1}} \left[\begin{array}{l} w_1\frac{\partial u}{\partial t} - Sw_1\left(\frac{\partial u}{\partial y}\right) + A_1\frac{\partial w_1}{\partial y}\frac{\partial u}{\partial y} - 2k^2 w_1 v - \\ A_2(Grw_1\theta + Gcw_1 C)\cos(\alpha) + A_3 w_1\left[M^2 + \frac{1}{K}\right]u \end{array}\right]dy - \left[w_1\left(\frac{\partial u}{\partial y}\right)\right]_{y_e}^{y_{e+1}} = 0 \tag{21}$$

$$\int_{y_e}^{y_{e+1}} \left[w_2\frac{\partial v}{\partial t} - Sw_2\left(\frac{\partial v}{\partial y}\right) + A_1\frac{\partial w_2}{\partial y}\frac{\partial v}{\partial y} + 2k^2 w_2 u - A_3 w_2\left[M^2 + \frac{1}{K}\right]v\right]dy - \left[w_2\left(\frac{\partial v}{\partial y}\right)\right]_{y_e}^{y_{e+1}} = 0 \tag{22}$$

$$\int_{y_e}^{y_{e+1}} \left[\begin{array}{l} w_3 \dfrac{\partial \theta}{\partial t} - Sw_3 \left(\dfrac{\partial \theta}{\partial y} \right) - A_4 \left(\dfrac{\partial w_3}{\partial y} \right) \left(\dfrac{\partial \theta}{\partial y} \right) - \\ Du \left(\dfrac{\partial w_3}{\partial y} \right) \left(\dfrac{\partial C}{\partial y} \right) \end{array} \right] dy - \left[w_3 \left(\frac{\partial \theta}{\partial y} \right) + Duw_3 \frac{\partial C}{\partial y} \right]_{y_e}^{y_{e+1}} = 0 \tag{23}$$

$$\int_{y_e}^{y_{e+1}} \left[\begin{array}{l} w_4 \dfrac{\partial C}{\partial t} - Sw_4 \left(\dfrac{\partial C}{\partial y} \right) + \dfrac{1}{Sc} \left(\dfrac{\partial w_4}{\partial y} \right) \left(\dfrac{\partial C}{\partial y} \right) + Krw_4 C \\ Sr \left(\dfrac{\partial w_4}{\partial y} \right) \left(\dfrac{\partial \theta}{\partial y} \right) \end{array} \right] dy - \left[w_4 \left(\frac{\partial C}{\partial y} \right) + Srw_4 \frac{\partial \theta}{\partial y} \right]_{y_e}^{y_{e+1}} = 0 \tag{24}$$

Assuming the form of approximate solution over a typical finite element

The finite element model may be obtained from equations (18)-(20) by substituting finite element approximations of the form:

$$u = \sum_{j=1}^{2} u_j^e \psi_j^e,\ v = \sum_{j=1}^{2} v_j^e \psi_j^e,\ \theta = \sum_{j=1}^{2} \theta_j^e \psi_j^e \ and \ C = \sum_{j=1}^{2} C_j^e \psi_j^e \tag{25}$$

With $w_1 = w_2 = w_3 = w_4 = \psi_j^e\ (i = 1,\ 2)$, where $u_j^e,\ v_j^e,\ \theta_j^e \ and \ C_j^e$ are the velocity in the direction of x-axis, y-axis, temperature and concentration respectively at the j^{th} node of typical e^{th} element $(y_e,\ y_{e+1})$ and ψ_i^e are the shape functions for this element $(y_e,\ y_{e+1})$ and are taken as:

$$\psi_1^e = \frac{y_{e+1} - y}{y_{e+1} - y_e} \ and \ \psi_2^e = \frac{y - y_e}{y_{e+1} - y_e},\ y_e \le y \le y_{e+1} \tag{26}$$

Derivation of finite element equations by substituting the approximate solutions into variational formulation

By choosing these functions equations (25)-(26) into equations (21)-(24) gives rise to the local stiffness matrices $\{[K^{mn}], [M^{mn}]\}$ and $\left\{\{u^e\},\ \{v^e\},\ \{\theta^e\},\ \{C^e\}, \{u'^e\},\ \{v'^e\},\ \{\theta'^e\}, \{C'^e\} \ and \ \{b^{me}\}\right\}$ $(m,n = 1,2,3,4)$. These matrices of order 2×2 and 2×1 and *prime* $(')$ indicates $\frac{\partial}{\partial y}$.

Therefore, the finite element model of the equations for e^{th} element thus formed is given by:

$$\begin{bmatrix} [K^{11}] & [K^{12}] & [K^{13}] & [K^{14}] \\ [K^{21}] & [K^{22}] & [K^{23}] & [K^{24}] \\ [K^{31}] & [K^{32}] & [K^{33}] & [K^{34}] \\ [K^{41}] & [K^{42}] & [K^{43}] & [K^{44}] \end{bmatrix} \begin{bmatrix} \{u^e\} \\ \{v^e\} \\ \{\theta^e\} \\ \{C^e\} \end{bmatrix} + \begin{bmatrix} [M^{11}] & [M^{12}] & [M^{13}] & [M^{14}] \\ [M^{21}] & [M^{22}] & [M^{23}] & [M^{24}] \\ [M^{31}] & [M^{32}] & [M^{33}] & [M^{34}] \\ [M^{41}] & [M^{42}] & [M^{43}] & [M^{44}] \end{bmatrix} \begin{bmatrix} \{u'^e\} \\ \{v'^e\} \\ \{\theta'^e\} \\ \{C'^e\} \end{bmatrix} = \begin{bmatrix} \{b^{1e}\} \\ \{b^{2e}\} \\ \{b^{3e}\} \\ \{b^{4e}\} \end{bmatrix} \tag{27}$$

These matrices are defined as follows:

$$\begin{cases} K_{ij}^{11} = -S\int_{y_e}^{y_{e+1}}\left[(\psi_i^e)\left(\frac{\partial\psi_j^e}{\partial y}\right)\right]dy + A_1\int_{y_e}^{y_{e+1}}\left[\left(\frac{\partial\psi_i^e}{\partial y}\right)\left(\frac{\partial\psi_j^e}{\partial y}\right)\right]dy + A_3\left(M^2+\frac{1}{K}\right)\int_{y_e}^{y_{e+1}}\left[(\psi_i^e)(\psi_j^e)\right]dy, \\ K_{ij}^{12} = -2k^2\int_{y_e}^{y_{e+1}}(\psi_i^e)(\psi_j^e)dy, K_{ij}^{13} = -GrA_2\cos(\alpha)\int_{y_e}^{y_{e+1}}(\psi_i^e)(\psi_j^e)dy,\ K_{ij}^{14} = -GcA_2\cos(\alpha)\int_{y_e}^{y_{e+1}}(\psi_i^e)(\psi_j^e)dy, \\ M_{ij}^{11} = \int_{y_e}^{y_{e+1}}(\psi_i^e)(\psi_j^e)dy, M_{ij}^{12} = M_{ij}^{13} = M_{ij}^{14} = 0, \end{cases}$$

$$\begin{cases} K_{ij}^{22} = -S\int_{y_e}^{y_{e+1}}\left[(\psi_i^e)\left(\frac{\partial\psi_j^e}{\partial y}\right)\right]dy + A_1\int_{y_e}^{y_{e+1}}\left[\left(\frac{\partial\psi_i^e}{\partial y}\right)\left(\frac{\partial\psi_j^e}{\partial y}\right)\right]dy + A_3\left(M^2+\frac{1}{K}\right)\int_{y_e}^{y_{e+1}}\left[(\psi_i^e)(\psi_j^e)\right]dy, \\ K_{ij}^{21} = 2k^2\int_{y_e}^{y_{e+1}}(\psi_i^e)(\psi_j^e)dy, K_{ij}^{23} = 0,\ K_{ij}^{23} = 0,\ K_{ij}^{24} = 0 \\ M_{ij}^{22} = \int_{y_e}^{y_{e+1}}(\psi_i^e)(\psi_j^e)dy, M_{ij}^{21} = M_{ij}^{23} = 0, \end{cases}$$

$$\begin{cases} K_{ij}^{31} = 0, K_{ij}^{32} = 0, \\ K_{ij}^{33} = -S\int_{y_e}^{y_{e+1}}\left[(\psi_i^e)\left(\frac{\partial\psi_j^e}{\partial y}\right)\right]dy + A_4\int_{y_e}^{y_{e+1}}\left[\left(\frac{\partial\psi_i^e}{\partial y}\right)\left(\frac{\partial\psi_j^e}{\partial y}\right)\right]dy, K_{ij}^{34} = -Du\int_{y_e}^{y_{e+1}}(\psi_i^e)\left(\frac{\partial\psi_i^e}{\partial y}\right)\left(\frac{\partial\psi_j^e}{\partial y}\right)dy, \\ M_{ij}^{31} = 0,\ M_{ij}^{32} = 0, M_{ij}^{33} = \int_{y_e}^{y_{e+1}}(\psi_i^e)(\psi_j^e)dy, M_{ij}^{34} = 0 \end{cases}$$

$$\begin{cases} K_{ij}^{41} = 0, K_{ij}^{42} = 0,\ K_{ij}^{43} = -Sr\int_{y_e}^{y_{e+1}}(\psi_i^e)\left(\frac{\partial\psi_i^e}{\partial y}\right)\left(\frac{\partial\psi_j^e}{\partial y}\right)dy, \\ K_{ij}^{33} = -S\int_{y_e}^{y_{e+1}}\left[(\psi_i^e)\left(\frac{\partial\psi_j^e}{\partial y}\right)\right]dy + \frac{1}{Sc}\int_{y_e}^{y_{e+1}}\left[\left(\frac{\partial\psi_i^e}{\partial y}\right)\left(\frac{\partial\psi_j^e}{\partial y}\right)\right]dy + Kr\int_{y_e}^{y_{e+1}}(\psi_i^e)(\psi_j^e)dy, \\ M_{ij}^{41} = 0,\ M_{ij}^{42} = 0, M_{ij}^{44} = \int_{y_e}^{y_{e+1}}(\psi_i^e)(\psi_j^e)dy, M_{ij}^{43} = 0 \end{cases}$$

$$\begin{cases} b_i^{1e} = \left[\left(\psi_i^e \right) \left(\dfrac{\partial u}{\partial y} \right) \right]_{y_e}^{y_{e+1}}, \; b_i^{2e} = \left[\left(\psi_i^e \right) \left(\dfrac{\partial v}{\partial y} \right) \right]_{y_e}^{y_{e+1}}, \\ b_i^{3e} = \left[\left(\psi_i^e \right) \left(\dfrac{\partial \theta}{\partial y} \right) + Du \left(\psi_i^e \right) \left(\dfrac{\partial C}{\partial y} \right) \right]_{y_e}^{y_{e+1}}, b_i^{4e} = \left[\left(\psi_i^e \right) \left(\dfrac{\partial C}{\partial y} \right) + Sr \left(\psi_i^e \right) \left(\dfrac{\partial \theta}{\partial y} \right) \right]_{y_e}^{y_{e+1}} \end{cases}$$

About the authors

Thirupathi Thumma is working as an Assistant Professor of Mathematics in the Department of Mathematics, B V Raju Institute of Technology. Medak. He received MSc degree in mathematics. He has a tech degree in computer science and he is pursuing PhD in applied mathematics from GITAM University, India. His research interests include, fluid flow in porous media, heat and mass transfer, fluid dynamics, magnetohydrodynamics using nanofluids, micropolar fluids and boundary value problems. He has published research papers in in archival international journals. Thirupathi Thumma is the corresponding author and can be contacted at: thirupathi.thumma@gmail.com

Dr Ali J. Chamkha is a Professor and a Chairman of the Mechanical Engineering Department and Prince Sultan Endowed Chair for Energy and Environment at Prince Mohammad Bin Fahd University (PMU) in the Kingdom of Saudi Arabia. He earned his PhD in Mechanical Engineering from Tennessee Technological University, USA, in 1989. His research interests include multiphase fluid-particle dynamics, nanofluids dynamics and fluid flow in porous media, heat and mass transfer, magnetohydrodynamics and fluid-particle separation. He has served as an Associate Editor for many journals such as *ASME Journal of Thermal Science and Engineering Applications*, *International Journal of Numerical Method for Heat and Fluid Flow*, *Journal of Nanofluids*, *Journal of Applied Fluid Mechanics*, *International Journal for Micro scale and Nanoscale Thermal and Fluid Transport Phenomena* and others. He has authored and co-authored over 500 publications in archival international journals and conferences.

Dr Siva Reddy Sheri is an Associate Professor in the Department of Engineering Mathematics, GITAM University, Hyderabad campus, Hyderabad, India. He received his PhD in Mathematics. His current area of research interests includes fluid dynamics, magnetohydrodynamics and heat and mass transfer. He got major Research Project from University Grants Commission (UGC) [F.No:42-22/2013 (SR) letter dated 12-03-2013]. He has published more than 30 research papers in national/international journals of repute.